IOP Conf. Series: Materials Science and Engineering **1345** (2026) 012003 doi:10.1088/1757-899X/1345/1/012003

Investigating the impact of annealing and deformation on grain size, dislocation density and the performance of High Purity Aluminum Wire by EBSD.

Yang Guo[1], Johan Westraadt[1,2], Jin Kwon[1], Tushar Garg[1], Xianhao Zhang[1], Chris Kovacs[3], Xuan Peng[3], Matt Rindfleisch[3], Michael Sumption[1], E.W. Collings[1]

[1] The Ohio State University, Columbus, U.S.A
[2] Center for Electron Microscopy and Analysis (CEMAS), U.S.A
[3] Hyper Tech Research, Columbus, U.S.A

*E-mail: guo.2000@osu.edu

Abstract. It is essential to develop lightweight cables with low AC loss in the application of electric aviation. High Purity Aluminum (HPAL), which operates effectively at cryogenic temperature, has been developed to compete with superconductors especially in higher frequencies. HPAL, characterized by 99.999% aluminum purity, achieves a resistivity ratio (RR) up to 1000. It has minimal impurities, dislocations, and defects resulting in remarkably low resistivity at cryogenic temperatures, but at the same time, the mechanical properties of HPAL itself are inadequate for practical application. HyperTech Research developed a multi-stranded HPAL wire with Cu-Ni matrix and Nb barrier to provide sufficient mechanical support. However, we wish to explore the microstructure and performance of HPAL wire under strain due to tensile stress, thermal stress. In this study, we performed Electron Backscatter Diffraction (EBSD) analysis on various HPAL wires to evaluate the impact of tensile stress and annealing on grain size and dislocation density which influence RR. Four samples, including as-drawn, annealed, and tensile-deformed conditions, were prepared and characterized using EBSD and cryogenic resistance measurements. Our chosen recovery anneal was seen to lead to a significant increase in RR (from 391 to 530) for our samples. Conversely, tensile deformation reduced the RR (from 530 to 277). Direct observation of changes in dislocation density analysis was not possible, but this may be possible with better surface preparation, and more aggressive recovery anneals. These results highlight the importance of material heat and mechanical treatment to enhance cryogenic electrical performance, with implications for HPAL use in high-frequency, cryogenically cooled power systems such as electric aircraft propulsion.

1. Introduction

The development of high-power density and simultaneously high efficiency power trains, including motors, generators, power electronics and electrical power cables and busbars is crucial for electric aviation[1–3]. Aluminum, as a lightweight and highly conductive material, has been considered for stator winding in electric aviation to achieve higher power density, particularly in cryogenically cooled systems [4,5]. However, conventional aluminum alloys still exhibit significant ohmic losses, generating substantial heat when carrying current, which limits their effectiveness as stator or rotor windings.

To overcome this, high-purity aluminum (HPAl) with a very high resistivity ratio (RR) offers a promising alternative due to its exceptionally low electrical resistivity at cryogenic temperatures. However, the material softness of HPAL makes it a challenge to apply in real application. Early research to strengthen the HPAL utilizing an Al-Fe-Ce sheath was successful[6,7]. However, an important problem was raised because this sheath had a moderately low resistivity that generated a significant "anomalous magnetoresistance" in the composite, due to Hall effect around the sheath [8].

To address both the mechanical weakness of pure aluminum and the magnetoresistance issue of Al-Fe-Ce sheath HPAL composite, HyperTech Research has developed HPAL composites, which consist of 99.999% aluminum filaments surrounded by Nb diffusion barriers and embedded within a Cu-Ni alloy matrix as shown in Figure 1a. These composites offer excellent mechanical support while preserving the electrical benefits of high-purity aluminum. They exhibit low AC losses and high RR at 20 K, which is liquid hydrogen temperature, a strong candidate of electric aviation fuel for next generation, especially within the 300–1000 Hz frequency range, making them strong candidates for stator coils in high-speed cryo-cooled generators and motors. They outperform MgB2 and ReBCO conductors in that frequency range[9,10]. A comparative study by Kwon demonstrated that although MgB_2 is a superconductor, its significant hysteresis losses under high-frequency AC operation make it less competitive than high-RR, multifilamentary aluminum-based conductors (termed "hyperconductors") at cryogenic temperatures [11].

Despite these advantages, HPAL conductors face a key challenge: in real motor applications, they are subject to cyclic Lorentz forces during operation, especially when used in stator or rotor windings. Given high purity aluminum's inherent softness, these forces can induce plastic deformation, leading to dislocation accumulation and grain refinement—both of which increase electrical resistivity. Since grain size and dislocation density are factors in determining the residual resistivity of high-purity materials at cryogenic temperatures, understanding how these microstructural features evolve under thermal and mechanical stress is essential [12–14].

In this study, we investigate the effects of annealing and tensile deformation on the microstructure of HyperTech-fabricated HPAL composites using Electron Backscatter Diffraction (EBSD). Our goal is to characterize how mechanical and thermal treatments affect the grain structure and dislocation density in HPAL. Samples were prepared in both cross-sectional and longitudinal orientations to enable a comprehensive EBSD analysis.

2. Sample preparation

2.1 sample with different heat treatment and tensile stressed condition

Four different HPAL samples were fabricated by Hyper Tech Research, with details listed in Table 1. Sample 4378 served as the control sample and did not undergo any heat treatment after wire drawing. The wire contains 36 HPAL filaments, each surrounded by a Nb barrier designed to

prevent diffusion, which could degrade the high-purity aluminum. A Cu-Ni alloy matrix was used to enhance the mechanical properties of the composite. Sample 4354 underwent heat treatment at 220°C for 5 hours, potentially annealing the aluminum and improving its RR. Sample 4354T refers to the same type of HPAL sample annealed at 220°C for 5 hours but subsequently subjected to tensile testing, the yielded part of the wire was taken as the sample 4354T. Sample 4363 has a higher aluminum content but did not receive any heat treatment after wire drawing. The fill factors of each component in the sample, diameter, annealing and stress conduction were shown in the Table.

Table 1. Samples sequence and detailed information of them

Sample#	Filaments: *5N Al (%)	Barrier: Nb (%)	Matrix: Cu-Ni (%)	Diameter (mm)	Annealing temperature/time	Stress condition
4378	22	27	51	0.63	No heat treatment	No
4354	27	24	49	0.84	220℃, 5$hours$	No
4354T	27	24	49	0.82	220℃, 5$hours$	Yielded
4363	31	36	33	0.56	No heat treatment	No

*5N Al: 99.999% Aluminum

2.2 Electropolishing

Due to the softness of high-purity aluminum and the complexity of our sample surfaces, electro-polishing was employed to achieve surface quality for EBSD[15]. First, the samples were attached horizontally and vertically to brass blocks using silver paste and subsequently cold-mounted using epoxy. Samples were then mechanically ground until both cross-sectional and longitudinal views were sufficiently exposed. Then electro-polishing was conducted using the LectroPol-5 electron-polishing machine (Struers) with an A2 electrolyte solution composed of 90 ml distilled water, 730 ml ethanol, 100 ml butoxyethanol, and 78 ml perchloric acid. A voltage of 15 V was applied for 25 seconds, effectively removing scratches and clearly exposing the high-purity aluminum components. Figure 1a shows an optical microscope image of the cross-sectional view of sample 4378 after mechanical grinding. Figures 1b and 1c illustrate the cross-sectional and longitudinal views after electro-polishing, respectively, of sample 4363. We noticed that the scratches were removed and the shinning aluminum parts were exposed after the electro-polishing.

3. Experimental approach

3.1 Electron Backscattered Diffraction (EBSD)

EBSD provides direct spatial and crystallographic insights into material features by analyzing diffraction patterns (Kikuchi patterns). Data were collected at 20 kV and 20 nA with a step size of 1 μm and 4x4 binning. Processing employed Nearest Neighbour Pattern Averaging Reconstruction (NPAR) and Spherical Indexing (bandwidth 127, SHI127), utilizing a critical misorientation angle of 5° for grain reconstruction. All maps were exported with an overlaid confidence index following reindexing. The grain size and misorientation were analyzed by OIM analysis 9. The grain size was calculated by how much of the total scanned area is occupied by grains of a particular size range[16]. Kernal Average Misorientation (KAM) measured the average misorientation angle

between pixel and its neighbor pixel, which reflects local lattice curvature, refers to dislocation density.

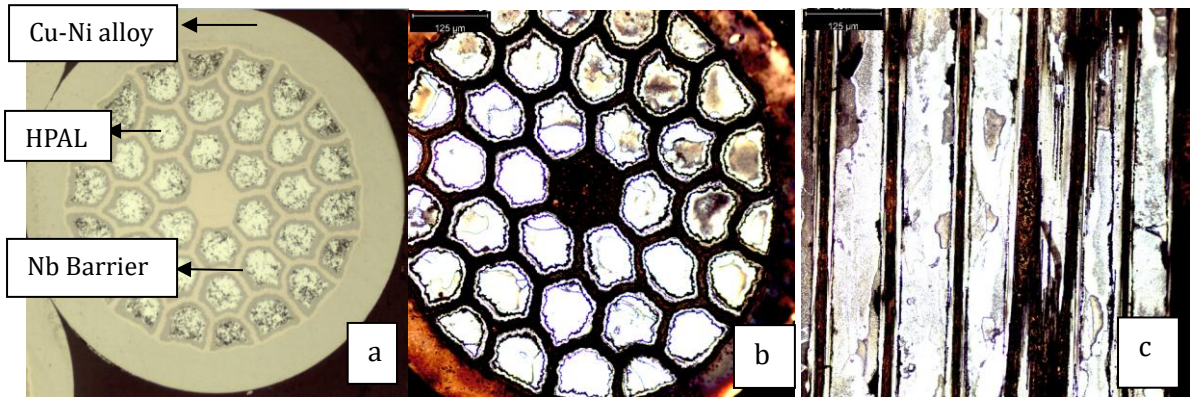

Figure 1: a) Optical microscope image of the cross-sectional view of sample 4378 after mechanical grinding. b) The cross-sectional view of sample 4363 after electro-polishing. c) The longitudinal view of sample 4363 after electro-polishing.

3.2 RR measurement

The samples were tested in a small conduction-cooled cryostat to measure their electrical resistance from 273 K down to 20 K. Each sample was placed inside a small vacuum chamber with multi-layer insulation (MLI), which was evacuated to create thermally insulated conditions. The samples were cooled by attaching them directly to the cryocooler's cold head. A thermocouple was attached to the samples to monitor and record temperature changes throughout the experiment. A four-point probe method was employed to measure the resistance of all HPAL samples. The samples were 5 cm long, and the current leads were attached at the sample ends. Voltage taps were attached to the center of each sample, using a gauge length of 2.5 cm. During measurements, a current of 1 A was applied, and the resulting voltage across each sample was recorded to calculate resistance. The RR was subsequently determined as the ratio of resistance at 273 K to resistance at 20 K.

4. Result

Figure 2a shows SEM images of the HPAL composite after electro-polishing. Figure 2b displays the inverse pole figure (IPF) of the multifilamentary high-purity aluminum in the cross-sectional view. Upon closer inspection, Figure 2c presents the IPF pattern of a single filament after filtering out low-confidence index (CI) regions. In these IPF maps, different colors correspond to different crystal lattice orientations, while similar colors indicate similar orientations. Figure 2d provides the IPF color key for aluminum, which aids in interpreting these orientation maps. We observed evidence of etching or oxidation at the aluminum filaments' edges, since the edges appear incomplete in the IPF patterns. It implies that the oxidization or etching happened and degraded surface quality and result in poor Kikuchi pattern quality, especially at the interface between aluminum filament and Nb barrier. An Energy Dispersive Spectroscopy (EDS) analysis will be performed to confirm the presence of aluminum oxide. The observed edge features are likely due to sample preparation process, rather than the annealing itself, as the annealing was conducted in an inert atmosphere. All samples are characterized cross-sectionally, but only sample 4378 was shown here because of the redundancy. While the cross-sectional view provides some insight, the

longitudinal view is more informative for analysing the impact of grain structure and dislocation density on electrical performance.

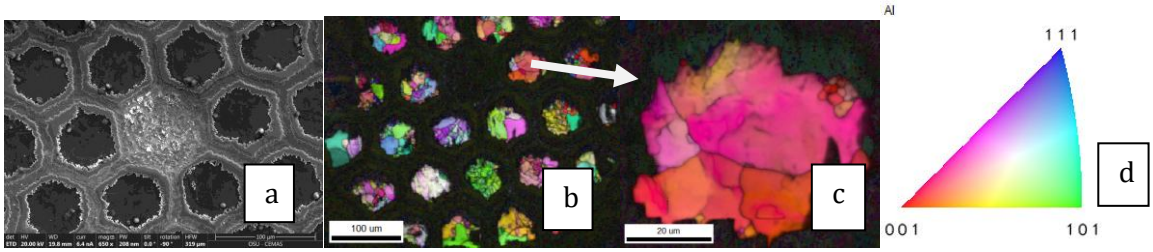

Figure 2: a) SEM imaging of sample 4378 (no heat treatment); b) Inverse Pole Figure (IPF) of sample 4378; c) IPF of one filament of sample 4378; d) IPF color key which the sample direction is [0 0 1] for aluminum (Parallel to the sample drawing direction).

Figure 3 shows the longitudinal IPF maps for all samples. The maps for samples 4354 and 4363 cover larger area of aluminum filament than that of sample 4378, owing to differences in surface preparation quality. Achieving uniform polishing was more challenging for sample 4378 because its lower aluminum filament fill factor made the surface more difficult to prepare consistently. We will improve polishing procedures in future work to ensure more comparable datasets. Overall, the drawn HPAL wires do not exhibit a strong, single crystallographic texture; multiple orientations are present in all cases. However, sample 4363 does contain a noticeable fraction of grains oriented close to the <001> direction. EBSD IPF-Z maps are referenced to the surface normal. For longitudinal sections, this direction is perpendicular to the drawing direction, while for cross sections it is parallel.

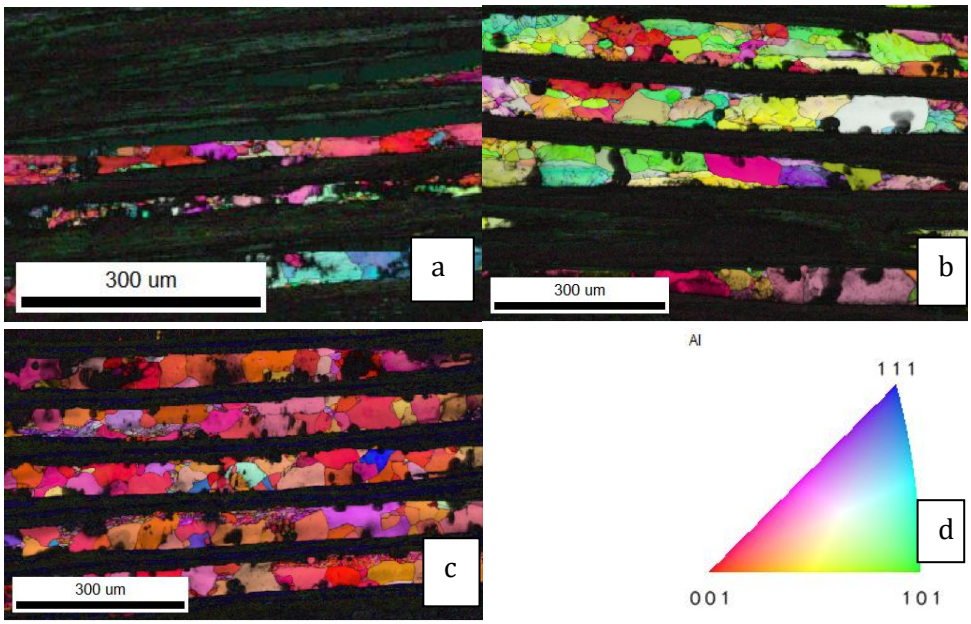

Figure 3: IPF patterns of all the sample longitudinally. a) Sample 4378 (as-drawn); b) Sample 4354 (220°C for 5 hrs); c) Sample 4363 (No heat treatment but larger fill factor of Al); d) IPF color key which the sample direction is [0 0 1] for aluminum (Normal to the sample drawing direction).

Figure 4 shows the KAM map for the longitudinal view of each sample. The green in the map represents the distortion of lattice density, which means, the greener, the more dislocation density inside of the grain. Because KAM is highly sensitive to local lattice distortion, the quality of the surface preparation plays a crucial role in data reliability. In our case, the complex and inconsistent surface condition after electro-polishing may have introduced some error or variability in the KAM data. Consequently, the grain size distribution and Kernel Average Misorientation (KAM) data from this sample may be biased or incomplete.

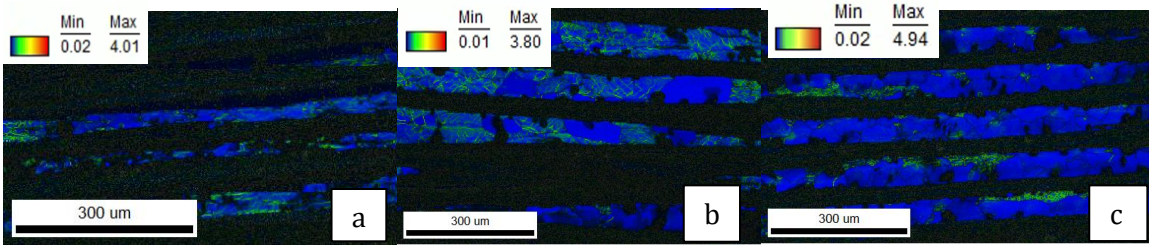

Figure 4: Kernal average misorientation (KAM) map of all the sample longitudinally. a) Sample 4378 (No heat treatment); b) Sample 4354 (220℃ for 5 hrs); c) Sample 4363 (No heat treatment but larger fill factor of Al).

Figure 5 presents the longitudinal grain size distributions of all four HPAL samples longitudinally, where x-axis is the diameter of the grain in micron, and y-axis is the area fraction of the grains. The average and standard deviation of the grain size of all samples are shown in Table 2. The as-drawn sample (4378) shows that it has the smallest size of grains on average compared to others. After annealing (sample 4354), the distribution shifts toward larger sizes, consistent with recovery and partial recrystallization. The tensile-tested sample (4354T) has slightly larger average value and standard deviation of grain size as the annealed one (sample 4354). In addition, larger Al filament size sample (4363) exhibits larger grain size than as drawn, but smaller than heat treated samples. Together, these distributions show that annealing and deformation both alter the grain size statistics of HPAL. While the present dataset is limited, additional sample analyses are planned to strengthen these observations.

Figure 6 shows the KAM distributions for the four HPAL samples longitudinally, where x-axis represents Kernal Average Misorientation (°), y-axis is number fraction (frequency). The as-drawn wire (4378) displays a relatively broad distribution with a peak around 0.17°, indicating higher local lattice curvature and dislocation content. Sample 4363, although also as drawn, has a narrower distribution with a lower peak (~0.07°), are likely due to differences in aluminum filament size. The interdiffusion between the HPAL filaments and the Nb barrier introduces dislocations in HPAL at the edge of the filaments. Larger HPAL filaments have lower surface-to-volume ratio, leading to a lower effective dislocation density, which agrees with the observed KAM distributions. After annealing (4354), the distribution narrows further (0.03°), reflecting recovery and partial recrystallization. The tensile-deformed sample (4354T) exhibits a right shift of KAM peak, suggesting heterogeneous plastic strain and increased local dislocation density. These comparisons show that annealing reduces lattice curvature while deformation increases it, and that even nominally similar as-drawn samples (4378 vs. 4363) can differ significantly in stored strain energy.

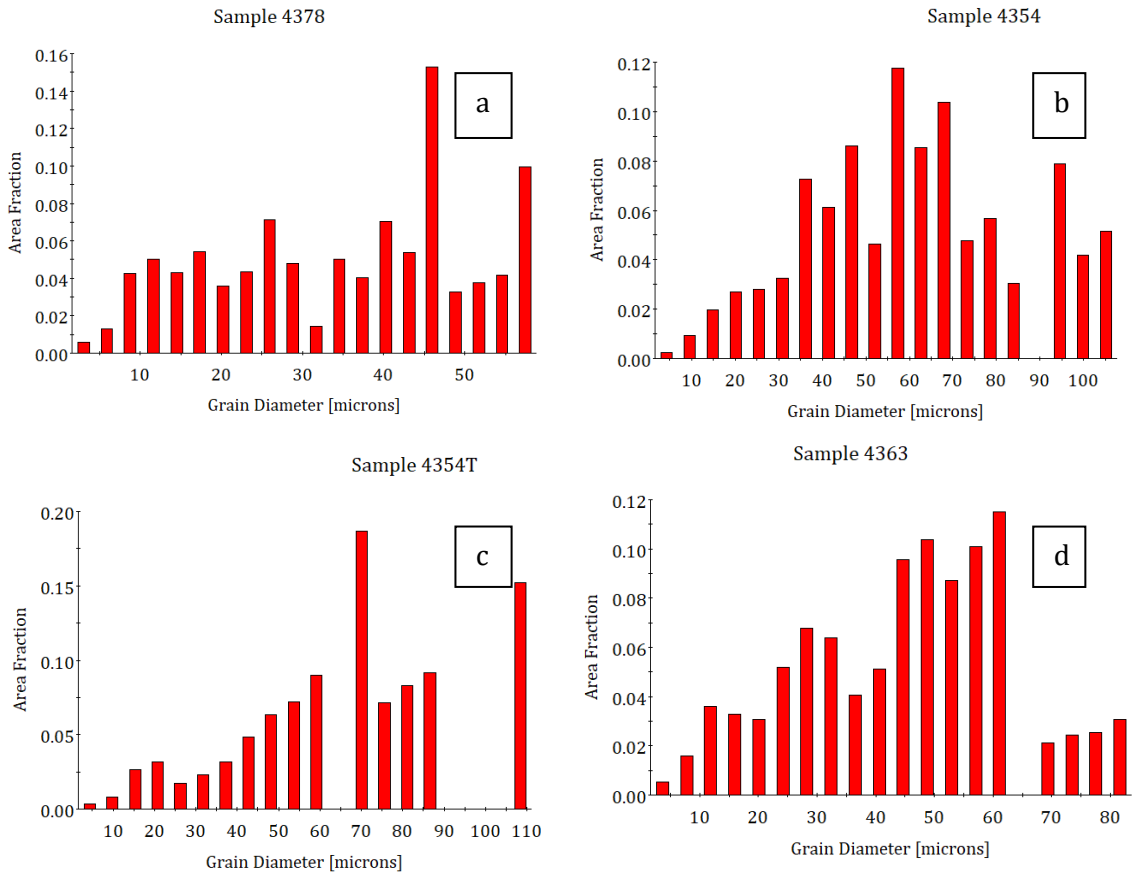

Figure 5. Grain size distribution along the longitudinal direction of all samples: a) Sample 4378 (No heat treatment); b) Sample 4354 (220℃ for 5 hrs); c) Sample 4354T (220℃ for 5 hrs, then plastic deformed); d) Sample 4363 (No heat treatment but larger fill factor of Al).

The RR measurements align with the expected trend. The as-drawn (unannealed) sample 4378 exhibited an RR of 280. After annealing, the RR increased significantly to 407 (sample 4354), indicating improved electron conduction at cryogenic temperatures because of RR recovery of annealing. Then, the sample that underwent tensile deformation showed a decreased RR of 214.5 in the yielded region. These results confirm our expectation that annealing enhances RR, while mechanical deformation degrades RR. The RR value obtained in this experiment is $RR_{Composite}$, which is affcted not only by the RR_{HPAl}, but also the fill factor λ, and RR of each material, and room temperature resistivity of each material in the composite[17]. The expression of $RR_{Composite}$ is shown as equation (1). The RR_{HPAl} can be back calcualted by our measured $RR_{Composite}$, assuming $RR_{Nb} = 20$, $RR_{Cu10Ni} = 1$, $\rho_{HPAl,ice} = 2.72 \times 10^{-8}\ \Omega \cdot m$, $\rho_{Nb,ice} = 1.4 \times 10^{-7}\ \Omega \cdot m$, $\rho_{Cu10Ni,ice} = 3.6 \times 10^{-7}\ \Omega \cdot m$.

$$RR_{Composite} = \frac{\left(\lambda_{HPAl} \Big/ \frac{\rho_{HPAl,ice}}{RR_{HPAl}} + \lambda_{Nb} \Big/ \frac{\rho_{Nb,ice}}{RR_{Nb}} + \lambda_{Cu10Ni} \Big/ \frac{\rho_{Cu10Ni,ice}}{RR_{Cu10Ni}}\right)}{\left(\lambda_{HPAl} \Big/ \rho_{HPAl,ice} + \lambda_{Nb} \Big/ \rho_{Nb,ice} + \lambda_{Cu10Ni} \Big/ \rho_{Cu10Ni,ice}\right)} \quad (1)$$

After the convertion from $RR_{Composite}$ to RR_{HPAl}, we can compare the RR_{HPAl} from sample to sample with the information of grain size distribution and Kernal Average Misorientation. Table 2 shows the comparison of average grain size, peak KAM, and $RR_{Composite}$ and RR_{HPAl}.

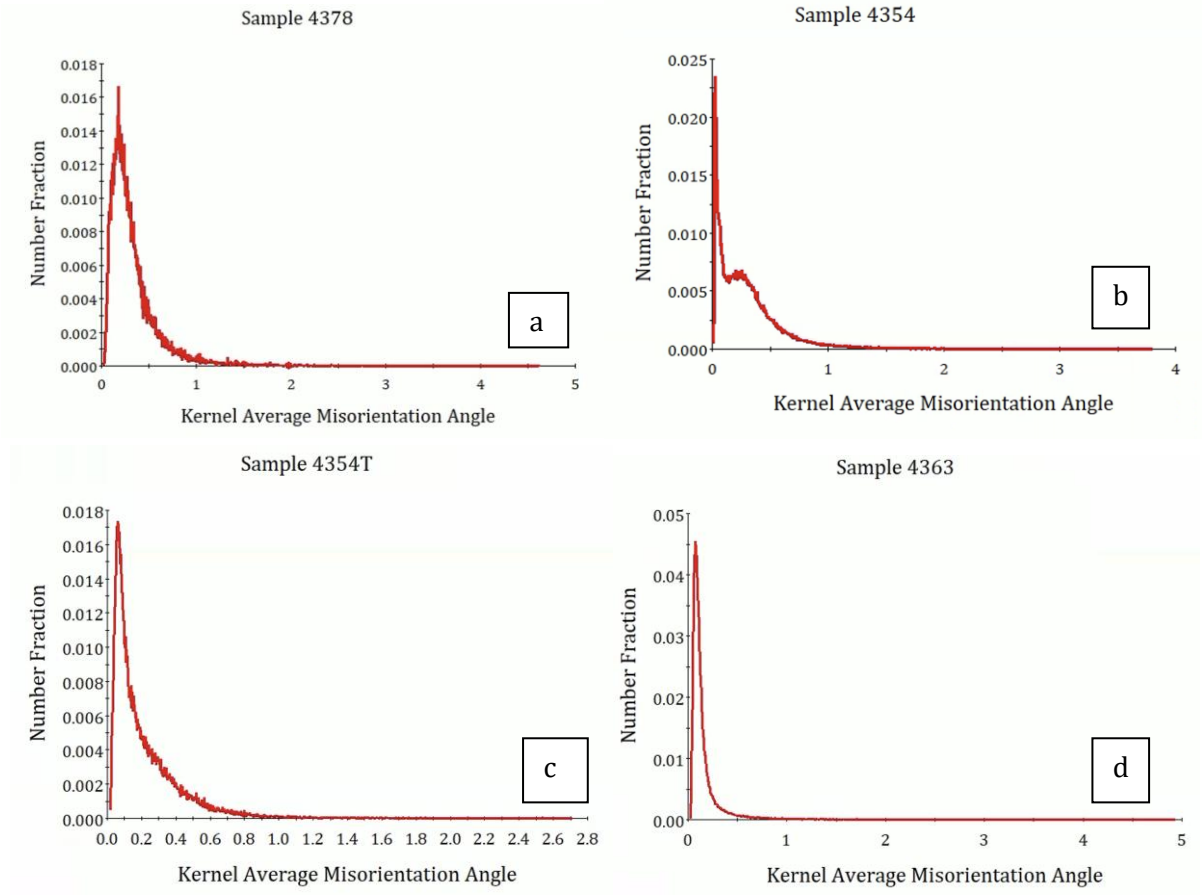

Figure 6. Kernal Average Misorientation distribution of all samples. . a) Sample 4378 (No heat treatment); b) Sample 4354 (220°C for 5 hrs); c) Sample 4354T (220°C for 5 hrs, then plastic deformed); d) Sample 4363 (No heat treatment but larger fill factor of Al).

5. Discussion

At cryogenic temperatures (20 K), the primary contributors to electrical resistivity in metals are dislocations and impurities, since phonon scattering is significantly suppressed at low temperature[18]. The recrystalliaztion temperature of pure aluminum is around 200°C for 2N grade and is 70 – 170 °C for 4N grade; for 5N grade aluminum it is expected to be even lower[19]. Since recovery precedes recrystallization, its onset temperature should be lower still. Thus, annealing at 220 °C effectively promotes both recovery and recrystallization in HPAL. Higher annealing temperatures are avoided because they would accelerate interdiffusion between the Nb barrier and HPAL, to degrade the high-purity aluminum filaments and reducing the residual resistivity ratio (RR). In this study, we looked to see how much recovery we get with annealing, and if we could observe a decrease in disolcations (via the KAM). We attempted to evaluate dislocation content using KAM from EBSD data. We do see the peak of KAM drops after the annealing, and increase after deformation, however, the correlation between KAM and RR was not

strong in our case. This could be attributed to surface preparation challenges, as KAM is highly sensitive to surface quality, particularly in electropolished samples.

Despite this limitation, our RR measurements clearly show that our recovery anneal does indeed increases RR, while yielding (plastic deformation) decreases it. While we were targeting a recovery, rather than grain growth or recystallization, EBSD analysis does suggest that our chosen anneal may increase grain size somewhat, although this is a secondary effect. It is important to clarify whether any artifacutal size effects are seen, where RR can be suppressed if the grain size gets near that of the mean free path. If this happens, it may complicate the data interpretation. To evaluate this, we calculated the electron mean free path λ using the equation:

$$\lambda = \frac{m v_F}{n e^2 \rho} \tag{2}$$

where m is the electron mass, v_F is the Fermi velocity, n is the conduction electron density, e is the elementary charge, and ρ is the resistivity at 20 K The mean free path represents the average distance an electron travels without scattering. Calculated values for each sample are summarized in Table 2. In all cases, the mean free path is approximately 10 times smaller than the average grain size. This suggests that grain boundaries are not small enough to modify (suppress) RR, and these effects can be ignored. This relationship implies that, unless the RR increases by an order of magnitude (e.g., 10×), grain size effect will not influence RR[20,21].

Table 2. Samples grain size, KAM, RR, mean free path comparison

Sample#	Average grain size,d (microns)	Peak Kernal Average Misorientation (degrees)	$RR_{Composite}$ (from 273K to 20K)	RR_{HPAl}(from 273K to 20K)	Mean free path λ (microns)	$K = \frac{d}{\lambda}$
4378 (No heat treatment)	34.78±15.53	0.1744	280	391	5.7	6.10
4354 (220 ℃ for 5 hours)	61.03±24.41	0.0273	407	530	7.8	7.82
*4354T (220 ℃ for 5 hours and plastic deformed)	*68.57±26.99	*0.0469	214.5	277	4.1	16.72
4363 (No heat treatment)	45.12±18.20	0.0740	308.5	398	5.8	7.78

*The sample only has one good filament for EBSD, the result might have bias.

6. Conclusion

In this study, we investigated the impact of annealing and deformation on RR, grain size, and dislocation density in high-purity aluminum (HPAL) composites fabricated by Hyper Tech Research. Using EBSD analysis and cryogenic RR measurements, we examined the effects of annealing and tensile deformation on grain structure and RR.

Our results show that our recovery anneal indeed increases the RR , tensile deformation leads to a notable decrease in RR. However, we could not directly observe changes in dislocation density, likely due to limitations in EBSD surface preparation quality. In addition, we did not recognize an obvious texture even if the HPAL is highly cold worked in EBSD maps.

Overall, the findings confirm that annealing effectively enhances RR and induces beneficial microstructural changes, while plastic deformation reduces RR through mechanisms not fully resolved in the present data. Therefore, controlling microstructure is essential for optimizing the cryogenic electrical performance of HPAL composites in high-frequency power applications, such as electric aircraft propulsion.

7. Future work

While the present surface preparation method provided reasonably good EBSD results, several regions still exhibited poor indexing due to surface contamination. To improve data quality, post-electropolishing treatment using a VibroMet polisher is recommended to remove residual contaminants and enhance pattern quality. Additionally, more sections of each sample should be scanned to improve statistical reliability. Higher-quality EBSD datasets will enable more accurate quantitative analysis of grain size, grain boundary, and dislocation density. Future efforts should also include EBSD characterization of HPAL samples subjected to fatigue or cyclic mechanical loading, in order to better understand microstructural changes such as fatigue-induced grain evolution and dislocation accumulation under realistic service conditions.

Acknowledgments

This study is funded by NASA SBIR phase I

References

[1] Haran K S, Kalsi S, Arndt T, Karmaker H, Badcock R, Buckley B, Haugan T, Izumi M, Loder D, Bray J W, Masson P and Stautner E W, 2017, High power density superconducting rotating machines - Development status and technology roadmap, *Supercond Sci Technol* **30** 123002

[2] Sumption M D, Murphy J, Susner M and Haugan T, 2020, Performance metrics of electrical conductors for aerospace cryogenic motors, generators, and transmission cables, Cryogenics **111** 103171

[3] Brown G, 2011, Weights and Efficiencies of Electric Components of a Turboelectric Aircraft Propulsion System, *49th AIAA Aerospace Sciences Meeting including the New Horizons Forum and Aerospace Exposition (Reston, Virigina: American Institute of Aeronautics and Astronautics)*

[4] Guo Y, Majoros M, Cantemir C G, Kwon J, Kovacs C, Rindfleisch M, Tomsic M, Doll D, Sumption M and Collings E W, 2024, Experimental study of two-phase cryogenic cooling of aluminum stator conductors using a single slot test configuration, *IOP Conf Ser Mater Sci Eng* **1301** 012161

[5] Guo Y, Sumption M D, Cantemir C G, Kwon J, Kovacs C, Majoros M, Collings E, Tomsic M, Doll D and Rindfleisch M, 2024, Experimental Study of Two-Phase Cryogenic Cooling of Aluminum Stator Conductors Using a Multi-Slots Test Configuration, *AIAA AVIATION FORUM AND ASCEND 2024 (Reston, Virginia: American Institute of Aeronautics and Astronautics)*

[6] Ho J C, Oberly C E, Gegel H L, Griffith W M, Morgan J T, O'Hara W T and Prasad Y V R K, 1986, A New Aluminum-Base Alloy with Potential Cryogenic Applications, *Advances in Cryogenic Engineering Materials* (Boston, MA: Springer US) pp 437–42

[7] Ho J C, 1987, Composite aluminum conductors for pulsed power applications at hydrogen temperatures, *Proc. 5th IEEE Pulsed Power Conf* pp 627–9

[8] Eckels P W, Iyer N C, Patterson A, Male A T, Parker J H and Coltman J W, 1989, Magnetoresistance: the Hall effect in composite aluminium cryoconductors, *Cryogenics* **29** 748–52

[9] Kwon H J, Sumption M D, Haugan T J and Collings E, 2023, High Purity Aluminum in Cryogenic Motors for Electric Aircraft *AIAA AVIATION 2023 Forum (Reston, Virginia: American Institute of Aeronautics and Astronautics)*
[10] Kwon H J, Kovacs C, Haugan T J, Sumption M D and Collings E, 2024, AC Loss of Various Conductors for Power Cables, Busbars, Motor Windings in Cryogenic Electric Aircraft *AIAA AVIATION FORUM AND ASCEND 2024 (Reston, Virginia: American Institute of Aeronautics and Astronautics)*
[11] Kwon J, Rindfleisch M, Peng X, Tomsic M, Bullard T, Haugan T, Sumption M D and Collings E W ,2025, Comparison of the AC Loss of MgB2 Superconductors and HPAL Cryogenic Composites for Rotating Machine Applications, *IEEE Transactions on Applied Superconductivity* **35** 1–7
[12] Hartwig K T and DeFrese R J, 1990, Mechanical and Electrical Testing of Composite Aluminum Cryoconductors, *Advances in Cryogenic Engineering Materials (*Boston, MA: Springer US) pp 709–15
[13] Hartwig K. T. and Lumbis A and R J, 1990, Cyclic-Strain Resistivity in Pure Aluminum at 20 K, *Advances in Cryogenic Engineering Materials:* Part A ed F R Reed R. P. and Fickett (Boston, MA: Springer US) pp 725–32
[14] Hartwig K, Yuan G and Lehmann P, 1985, The effects of low temperature fatigue on the RRR and strength of pure aluminum, *IEEE Trans Magn* **21** 161–4
[15] Ma D, Li S and Liang C, 2009, Electropolishing of high-purity aluminium in perchloric acid and ethanol solutions *Corros Sci* **51** 713–8
[16] Mingard K P, Roebuck B, Bennett E G, Gee M G, Nordenstrom H, Sweetman G and Chan P, 2009, Comparison of EBSD and conventional methods of grain size measurement of hardmetals *Int J Refract Metals Hard Mater* **27** 213–23
[17] Kwon J, Rindfleisch M, Peng X, Tomsic M, Bullard T, Haugan T, Sumption M D and Collings E W, 2025, Comparison of the AC Loss of MgB2 Superconductors and HPAL Cryogenic Composites for Rotating Machine Applications, *IEEE Transactions on Applied Superconductivity* **35** 1–7
[18] Niewczas M and Bian Q, 2016, Influence of dislocation microstructure on low temperature magnetoresistance in copper single- and polycrystals *Mater Des* **96** 203–16
[19] Nagira T, Liu X, Ushioda K and Fujii H, 2021, Microstructural evolutions of 2n grade pure al and 4n grade high-purity al during friction stir welding, *Materials* **14** 3606
[20] Fickett F R, 1983, *Electrical Properties Materials at Low Temperatures* (ASM International) pp 163–201
[21] Fickett F R, 1971, Aluminum—1. A review of resistive mechanisms in aluminum, *Cryogenics* **11** 349–67